Supporting Information

Goulet et al. 10.1073/pnas.1319848111

SI Materials and Methods

Production and Labeling of Kinesin-5 Constructs. Cysteine-light human kinesin-5 (K5) motor domain (MD) constructs (residues 1–367) with a single cysteine on L5 (T126C) or on the neck-linker (NL) (V365C) were recombinantly expressed in *Escherichia coli* and purified using a C-terminal His_6-tag as previously described (1–3). We also generated a construct containing a cysteine in the N terminus (A9C) by chemical synthesis (GenScript), cloned into a pET21a expression vector. An undecagold cluster conjugated to a maleimide linker, provided by Dan Safer (University of Pennsylvania, Philadelphia), was used to label single cysteines (T126C, V365C, and A9C) covalently in the K5 constructs. Protocols for gold and protein activation and labeling of T126C and V365C were reported previously (3). The A9C K5 construct was exchanged into labeling buffer [10 mM Hepes (pH 7), 25 mM K-acetate, 1 mM Mg-acetate, 1 mM EGTA] supplemented with 1 mM Tris(2-carboxyethyl)phosphine (TCEP) (Sigma) using a PD10 desalting column (Amersham Biosciences). Eluted protein was incubated for 45 min at room temperature with 5 U/mL apyrase to remove bound nucleotides and recovered by nickel affinity chromatography. Immediately before mixing with a 40-fold molar excess of activated gold, the nucleotide-free A9C K5 construct was exchanged into labeling buffer without TCEP. After 18-h incubation at room temperature, labeled A9C proteins were recovered by nickel affinity chromatography. The labeling efficiency given by the concentrations of eluted protein and attached gold (determined by absorbance at 420 nm) was 64%.

We also generated two additional K5 MD constructs to monitor NL movement and the effect of deleting the N terminus on this process. The first construct, described previously (3), consists of a 1–367 monomeric construct containing two cysteines at positions 256 (V256C) and 365 (V365C). We previously showed that these mutations do not have any appreciable effect on the microtubule (MT)-activated ATPase k_{cat}. We also demonstrated in that study that attaching distance-sensitive fluorescent probes at these locations allows us to monitor the kinetics of nucleotide-induced NL movement, because the cysteine at position 256 is likely to serve as a stable frame of reference. In this study, we refer to this construct as "NT-Intact." The other construct is equivalent to the NT-Intact construct, except that the first 17 N-terminal residues have been deleted. We refer to this construct as "NT-Deleted." Both constructs were generated from inserts that were chemically synthesized (GenScript) and cloned into pET21a. Both constructs were labeled with tetramethyl rhodamine 5′ maleimide (TMR) by incubation for 24 h with a 10-fold molar excess of TMR over MD, followed by gel filtration on Sephadex G25 to remove unbound label. Labeling stoichiometries of 1.7–1.9 were achieved for both constructs.

Cryo-Electron Microscopy Image Analysis. Bovine brain tubulin (Cytoskeleton, Inc.), at a final concentration of 5 mg/mL, was incubated for 1.5 h at 37 °C in a buffer containing 100 mM MES (pH 6.5), 1 mM $MgCl_2$, 1 mM EGTA, 1 mM DTT, and 2 mM GTP. Polymerized MTs were stabilized with 1 mM paclitaxel (Calbiochem) in dimethyl sulfoxide for a further 1.5 h at 37 °C. K5 MD was dialyzed into 80 mM Pipes (pH 6.8), 5 mM $MgCl_2$, 1 mM EGTA, and 1 mM TCEP before incubation with ADP aluminum fluoride (ADP.AlFx), or into 20 mM Pipes (pH 6.8), 5 mM $MgCl_2$, 1 mM EGTA, and 1 mM TCEP before incubation with ADP. MTs (2 μM) were incubated at room temperature either with a 10-fold molar excess of K5 MD (20 μM) and 2 mM ADP/2 mM $AlCl_3$/7 mM NaF for 45 min or with a 15-fold excess of K5 MD (30 μM), preincubated for 5 min on ice with 10 mM ADP and 2.5% (wt/vol) glycerol for ∼30 s. Subsequently, 3.5 μL of the MT-MD mixture was applied to glow-discharged C-flat holey carbon grids (Protochips Inc.) at 24 °C and 100% humidity and was automatically blotted and plunged into liquid ethane (Vitrobot; FEI Company). Low-dose images were acquired using a Tecnai F20 FEG microscope (FEI Company) operating at 200 kV using a Gatan CT3500 Cryotransfer System (Gatan, Inc.). Micrographs were recorded at 0.7–2.4 μm defocus, 50,000× nominal magnification on Kodak SO-163 films digitized (SCAI scanner; Carl Zeiss, Inc) to a final sampling of 1.4 Å per pixel (ADP.AlFx) or at 68,000× magnification on a 4 k × 4 k CCD camera (Gatan) with a sampling of 2.2 Å per pixel (ADP).

3D reconstructions were produced using a previously described custom single-particle procedure (4, 5), which combines manual particle picking using Boxer (6), angle determination by projection matching using SPIDER (7), and angle refinement, 3D reconstruction, and full contrast transfer function correction using FREALIGN (8). MD bound to an αβ-tubulin dimer (139,000 and 125,000 asymmetric units) boxed from 167 and 213 13-protofilament MTs gave an isotropic angular distribution (Fig. S1 and Table S1) and was used to calculate the 3D reconstructions of the ADP.AlFx and ADP states, respectively. The resolution of the ADP.AlFx and ADP reconstructions was estimated at 9.2 Å and 10 Å, respectively, using the Fourier Shell Correlation 0.5 criterion. The occupancy of the disconnected NL electron microscopy density in the ADP.AlFx reconstruction was calculated from the ratio between the mean voxel values of this density and of a section of similar volume in the body of the MD (the helix α4 region).

The same reconstruction procedure was applied to the gold-labeled T126C (T126C-Au), V365C (V365C-Au), and A9C (A9C-Au). The presence of the gold cluster did not perturb the overall structure of K5 MDs, and gold densities were readily visible (Fig. S2). To extract gold-specific densities, difference maps were calculated between scaled and aligned gold-labeled and unlabeled reconstructions in each nucleotide state, each band-pass filtered at the same frequencies, using SPIDER (7) and IMAGIC-5 (9). We also prepared cryo-electron microscopy (cryo-EM) samples of the 5′adenylyl-β,γ-imidophosphate (AMPPNP) and rigor states using gold-labeled A9C following the procedure described in ref. 3. 3D reconstructions and difference maps were calculated as described above.

Atomic Model Building. The coordinates of αβ-tubulin dimer [Protein Data Bank (PDB) ID code 1JFF (10)] and of different conformations of human K5 MDs available in the PDB were rigidly fit into an asymmetric unit of the ADP.AlFx and ADP reconstructions using UCSF Chimera (11). The K5 MD coordinates with AMPPNP or ADP bound produced the highest cross-correlation (CC) value between the experimental and the model-based simulated maps and were used as starting model for the ADP.AlFx and ADP states, respectively (Table S2). However, because helix α4 is longer in our reconstruction than in the available ADP crystal structures, we modeled seven helical turns of helix α4 (residues D279–E304), as observed in the K5 AMPPNP crystal structure, in all our other reconstructions. Although almost identical CC values are obtained for MD models with a long (0.791) or a short (0.793) helix α4, the longer version is more consistent overall with our reconstructions and with the observation of a long helix α4 of constant length in all four nucleotide states of K1 MD reconstructions (5). Because of the

absence of well-defined density accounting for switch II loop in our ADP reconstruction, we did not model residues N271–K280, which also are missing in the available ADP crystal structures. The coordinates of αβ-tubulin/K5 MD complexes were refined by flexible fitting using Flex-EM (12). To avoid overfitting, the rigid bodies used in the first cycle of flexible fitting were defined using the server RIBFIND (13). In a second cycle, individual secondary structure elements were released.

After the overall conformation of the K5 MD in each nucleotide state was modeled, the conformations of the N terminus, L5, and NL in the MD were defined more precisely. These mechanochemical elements either are absent in the available K5 MD crystal structures or are in a conformation that does not match the EM density. Using Modeler (14, 15), we generated 500 conformers of the N terminus for the ADP.AlFx (11 amino acids, N6–G16) and the ADP (seven amino acids, A9–K15) states. The conformers in which A9 satisfied the constraint of the gold position were selected, and the final conformation depicted in both states is the one that gave the highest CC value. Similarly, the final conformation of L5 in between the two Pro residues P121 and P131 (N122–D130) was generated by Modeler and selected among 250 initial conformers according to the same criteria. Finally, the disconnected conformation of the NL in the ADP.AlFx state was calculated using a conjugate-gradient energy minimization approach implemented in Flex-EM; this method was applied to the complete MD model with the NL docked along the MD to sample its conformational space independently of the EM reconstruction. Among 100 conformations of the NL, 44 were selected in which V365C satisfies the gold-density position. Subsequent ranking of these models based on the CC value and rmsd clustering Cα cutoff of 0.35 Å produced four clusters. The first cluster, whose 31 members have the highest CC, represents the docked conformation; the second cluster encompasses nine conformations that fit into the EM density of the undocked conformation; the third cluster is close to the second; and the last conformer lies between the docked and undocked conformations (Fig. S3). The final ADP.AlFx and ADP models, in which the L5 and N terminus conformation cannot be refined further at the current resolution, were energetically minimized, and their stereochemistry was checked. The increase of CC values calculated with the initial and final models assesses the quality of the fit (Table S2).

Kinetic Methodologies. The MT-activated ATPase activities of the K5 constructs were determined by measuring phosphate production with a commercially available kit (EnzChek; Molecular Probes). Assays contained 25–50 nM MD and a minimum of a fivefold molar excess of MTs (Fig. S6).

We measured the kinetics of NL movement and of the effect of N-terminal deletion on NL movement by labeling the two cysteines in the NT-Intact and NT-Deleted constructs with TMR. We mixed TMR-labeled MD complexes with a three- to fivefold molar excess of MTs by adding the two components together in buffer containing 50 mM potassium acetate, 25 mM Hepes, 5 mM magnesium acetate, 1 mM EGTA, 1 mM DTT (pH 7.50), and 0.2 U/mL type VII apyrase (Sigma-Aldrich) and incubating at 20 °C for 20 min before initiating the experiment. These samples then were mixed in a KinTek SF-2004 stopped-flow spectrophotometer with an instrument dead time of 1.2 ms. The TMR fluorophore was excited at 520 nm, and the fluorescence emission was monitored at 90° to the incident beam through a 590-nm long-pass filter to monitor changes in TMR emission.

Gliding Assay and Image Acquisition. The gliding assay was done in a flow cell (microscope slide plus hydrophobic coverslip, separated with double-sided tape). Initially, the flow cell was filled with penta-His antibodies (200 μg/mL; Qiagen) at 20 μg/mL (2.5 μL antibody and 22.5 μL PEM80); after a 10-min absorption the surface was blocked for 10 min by adding a casein solution (5.55 mg/mL of casein in 35 mM Pipes, 5 mM $MgSO_4$, 1 mM EGTA, 0.5 mM EDTA). Next motors were added [in 80 mM Pipes (pH 6.9), 50 mM CH3CO2K, 4 mM $MgSO_4$, 1 mM DTT, 1 mM EGTA, 10 μM paclitaxel, 1 mg/mL casein] and were incubated for 5 min to bind the motors specifically to the antibodies by their His-tags. Finally, 1 μL of fluorescent MTs [30% rhodamine-tubulin (Cytoskeleton Inc, # T331) and 70% nonfluorescent tubulin] was added in 50 μL of motility buffer with 0.6 mM (Fig. 4*B*) or 1 mM (Fig. S7) ATP and an oxygen-scavenging system (250 μg/mL glucose oxidase, 30 μg/mL catalase, 4.5 mg /mL glucose).

Motion of the MTs was monitored using an inverted microscope (TE2000; Nikon) with a 100× objective (NA = 1.49). Fluorescence images were acquired at 11.8 frame/s (FPS) using an EMCCD camera (Quantem 512SC; Photometrics; 512 × 512 imaging pixels) and μ-Manager software; one pixel corresponded to 60 nm. Movies were composed of 500 images. To track the fluorescent MTs, images first were processed with Matlab to remove shot noise and to enhance the visibility of MTs. Then, the intensity profile of the MT from each frame was determined using ImageJ. After smoothing the intensity profile first with a median filter (five points) and then with a Loess filter, we determined the tip position of MT in each frame from the point where the intensity from median filter and Loess filter became the same. This method yielded an uncertainty in the location of the MT tip of approximately one pixel, likely accounting for some of the "waviness" apparent in the trajectories. Finally, we smoothed each trajectory with a median filter (20 points). In some trials, a fraction (~30%) of the NT-Deleted (but not NT-Intact) MTs was paused on the coverslip, but in other trials only a few in each group were paused. Paused MTs and MTs exhibiting stop-and-go motion were excluded from the analysis (three such NT-Deleted traces were excluded, from 25 overall) in which individual trajectories were averaged together.

1. Rosenfeld SS, Xing J, Jefferson GM, King PH (2005) Docking and rolling, a model of how the mitotic motor Eg5 works. *J Biol Chem* 280(42):35684–35695.
2. Behnke-Parks WM, et al. (2011) Loop L5 acts as a conformational latch in the mitotic kinesin Eg5. *J Biol Chem* 286(7):5242–5253.
3. Goulet A, et al. (2012) The structural basis of force generation by the mitotic motor kinesin-5. *J Biol Chem* 287(53):44654–44666.
4. Sindelar CV, Downing KH (2007) The beginning of kinesin's force-generating cycle visualized at 9-A resolution. *J Cell Biol* 177(3):377–385.
5. Sindelar CV, Downing KH (2010) An atomic-level mechanism for activation of the kinesin molecular motors. *Proc Natl Acad Sci USA* 107(9):4111–4116.
6. Ludtke SJ, Baldwin PR, Chiu W (1999) EMAN: Semiautomated software for high-resolution single-particle reconstructions. *J Struct Biol* 128(1):82–97.
7. Frank J, et al. (1996) SPIDER and WEB: Processing and visualization of images in 3D electron microscopy and related fields. *J Struct Biol* 116(1):190–199.
8. Grigorieff N (2007) FREALIGN: High-resolution refinement of single particle structures. *J Struct Biol* 157(1):117–125.
9. van Heel M, Harauz G, Orlova EV, Schmidt R, Schatz M (1996) A new generation of the IMAGIC image processing system. *J Struct Biol* 116(1):17–24.
10. Löwe J, Li H, Downing KH, Nogales E (2001) Refined structure of alpha beta-tubulin at 3.5 A resolution. *J Mol Biol* 313(5):1045–1057.
11. Pettersen EF, et al. (2004) UCSF Chimera—a visualization system for exploratory research and analysis. *J Comput Chem* 25(13):1605–1612.
12. Topf M, et al. (2008) Protein structure fitting and refinement guided by cryo-EM density. *Structure* 16(2):295–307.
13. Pandurangan AP, Topf M (2012) Finding rigid bodies in protein structures: Application to flexible fitting into cryoEM maps. *J Struct Biol* 177(2):520–531.
14. Sali A, Blundell TL (1993) Comparative protein modelling by satisfaction of spatial restraints. *J Mol Biol* 234(3):779–815.
15. Fiser A, Do RK, Sali A (2000) Modeling of loops in protein structures. *Protein Sci* 9(9): 1753–1773.

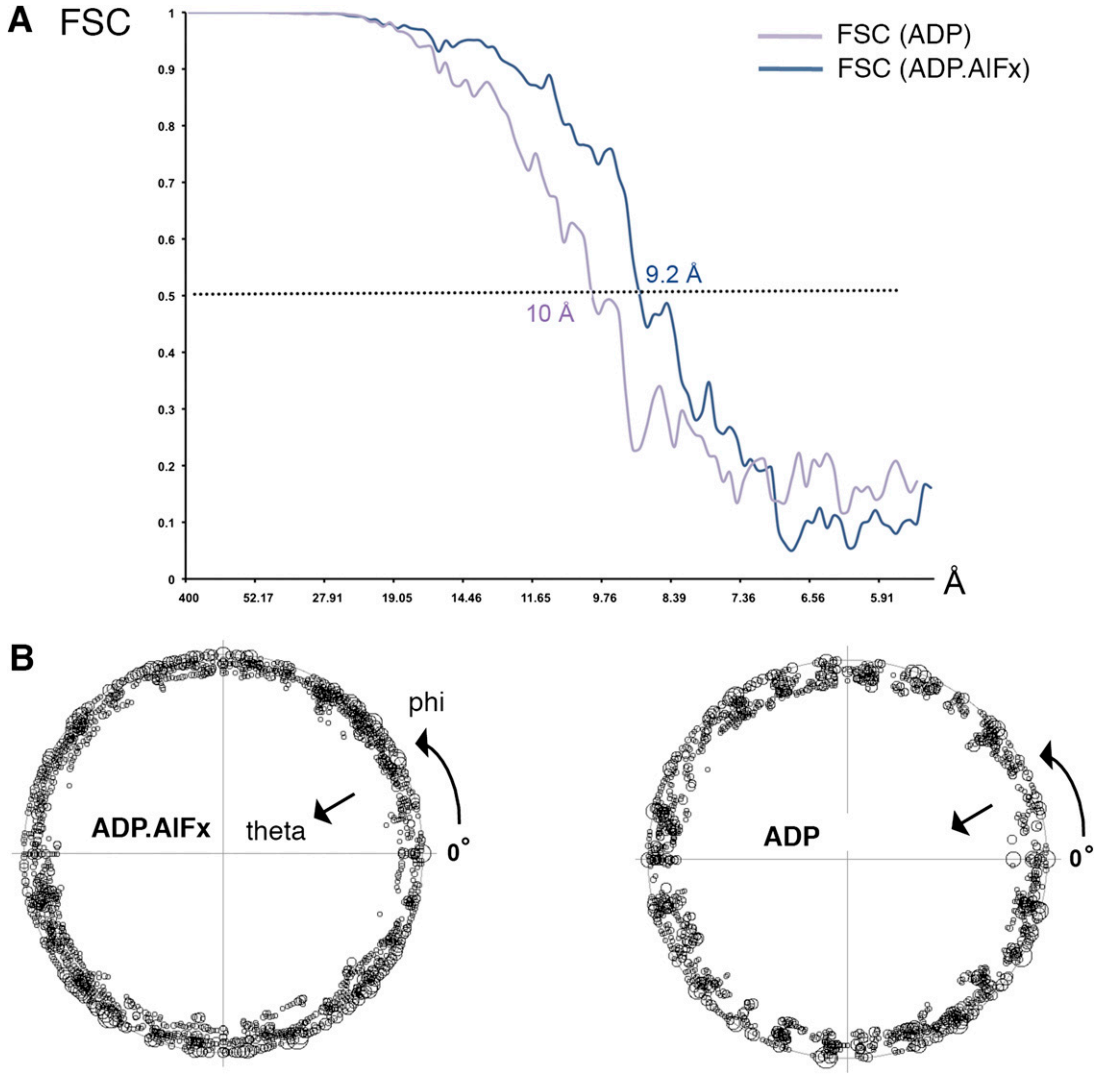

Fig. S1. Resolution and data angular distribution of the cryo-EM reconstructions. (*A*) Fourier shell correlation (FSC) curves computed between two independent reconstructions for ADP.AlFx (blue) and ADP (purple) states. The FSC 0.5 criterion indicates 9.2-Å and 10-Å resolution (dotted line). See also Table S1. (*B*) Angular distribution of the particles used for the ADP.AlFx and ADP reconstructions. The size of the small circles representing phi and theta angles is proportional to number of particle projections at that angle.

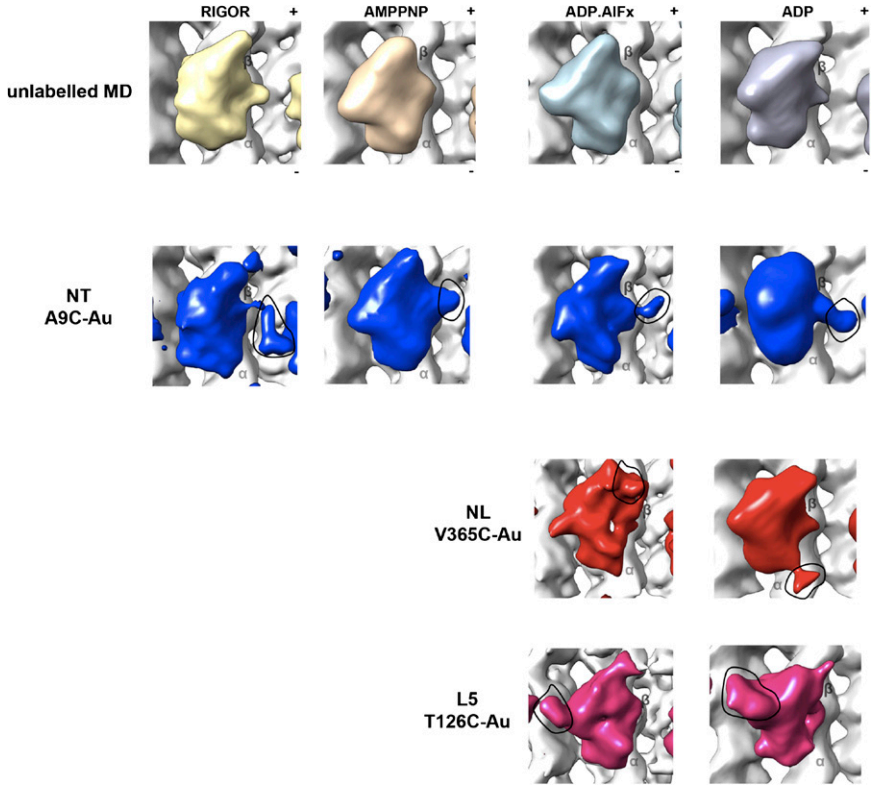

Fig. S2. Comparison between unlabeled and gold-labeled K5 MD reconstructions. Surface views of all K5 MD reconstructions in (from left to right) rigor, AMPPNP (from ref. 1), ADP.AlFx, and ADP states are shown. Unlabeled K5 MD reconstructions (*Top Row*) are filtered to match the lower resolution of the reconstructions calculated using gold-labeled K5 MD: A9C-Au in blue, V365C-Au in red, and T126C-Au in pink. Structures are band-pass filtered in the range of 30–16 Å (according to the final resolution; Table S1) and are contoured to account for the volume of the complex. Positions of gold densities in a single MD are outlined. The MT plus end is toward the top.

1. Goulet A, et al. (2012) The structural basis of force generation by the mitotic motor kinesin-5. *J Biol Chem* 287(53):44654–44666.

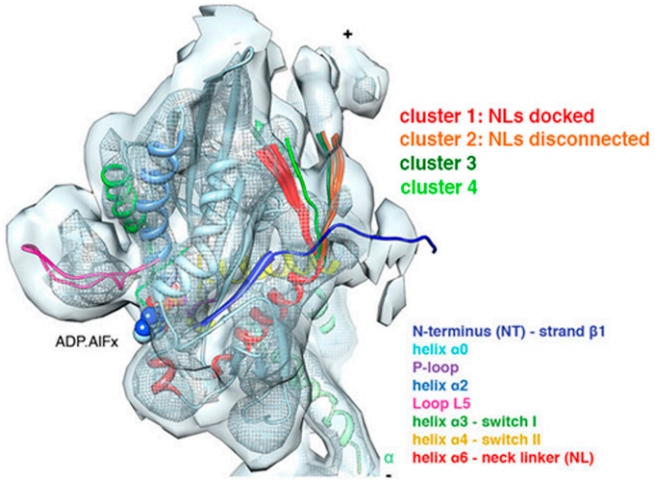

Fig. S3. Visualization of NL destabilization on initiation of ATP hydrolysis. Pseudoatomic models of human K5 MD (color-coded as in the key) bound to an αβ-tubulin dimer (green ribbon) docked into the ADP.AlFx cryo-EM reconstruction contoured as in Fig. 1. The 44 NL conformers produced by energy minimization that satisfy the gold density formed four clusters based on an rmsd Cα cutoff of 0.35 Å; two of these correspond to cluster 1, the docked NL conformation (red ribbons, 31 members), and cluster 2, the disconnected NL conformation (orange ribbons, nine members). The third cluster (dark green, three members) is close to the second, and the last conformer conformations (light green, one member) lies between the docked and undocked NLs.

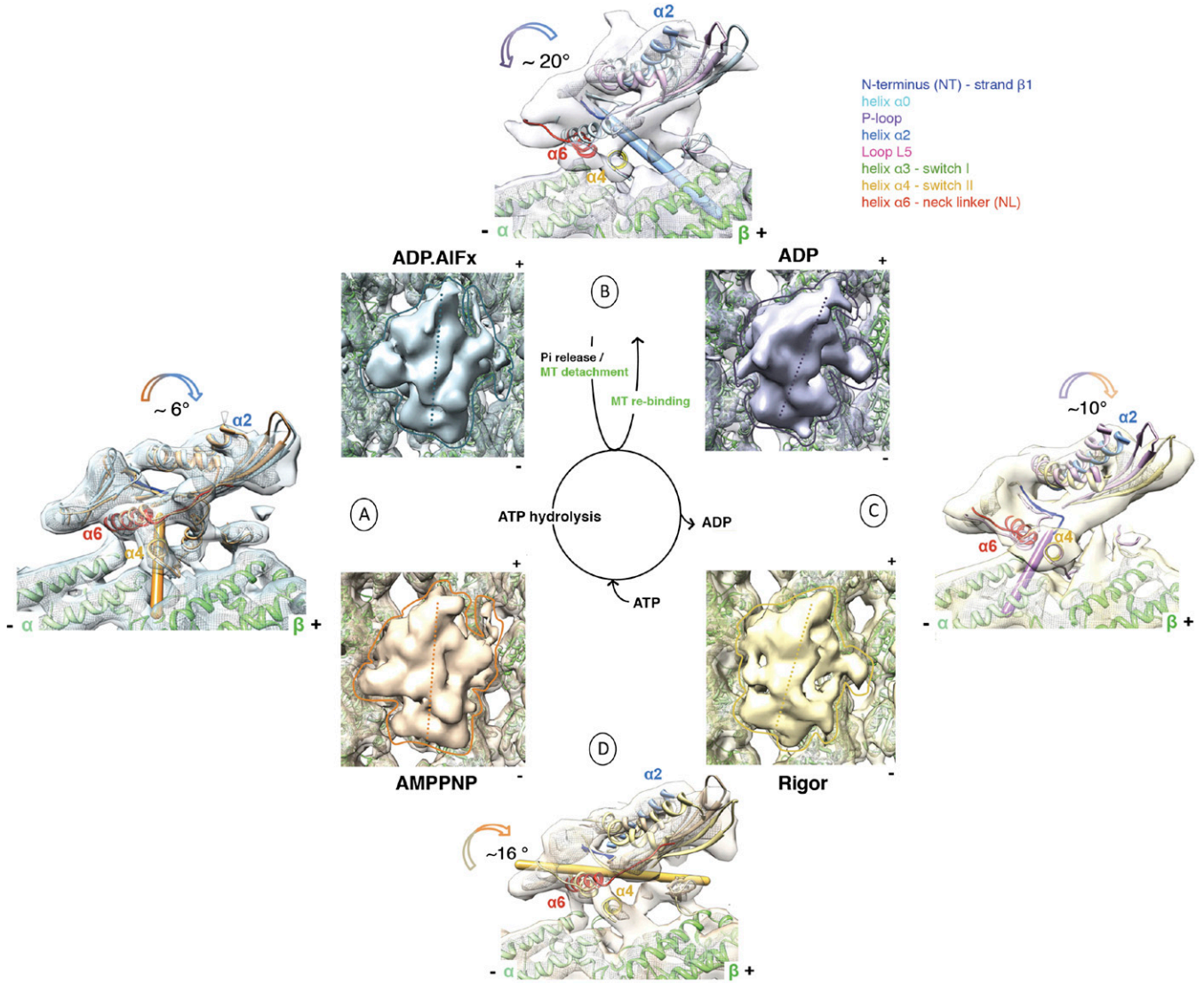

Fig. S4. Global movements of the human K5 MD during its MT-based ATPase cycle. The central schematic illustrates steps in the ATPase cycle with the associated conformational states: ATP hydrolysis (step A), Pi release/MT detachment and MT rebinding (step B), ADP release (step C), and ATP binding (step D). For each nucleotide state, front views of an αβ-tubulin dimer (green ribbon) with bound K5 MD are shown to illustrate the large-scale conformational changes that occur at each step: AMPPNP (coral); ADP.AlFx (blue); ADP (purple); and rigor (yellow). The MT plus end is toward the top, and K5 MDs are outlined. At the top, bottom, left, and right of the figure, conformational changes in the pseudoatomic coordinates (color-coded as in the key) at each step are compared and docked into the cryo-EM density. In these side views, the MT plus end is toward the right. The directions of MD rotations/tilts are indicated with color-coded arrows, and the rotational axis of each conformational change is indicated by a colored rod. Front-view reconstructions are displayed at a threshold equivalent to the molecular weight of the complex; side-view reconstructions are contoured at a higher threshold to show most clearly the rotations as follows: AMPPNP [surface contour: 1σ (front view) and 1.8σ (side view); mesh contour: 3σ]; ADP.AlFx [surface contour: 1.1σ (front view) and 2σ (side view), mesh contour: 3.25σ]; ADP [surface contour: 1.56σ (front view) and 2σ (side view), mesh contour: 3.4σ]; rigor [surface contour: 0.94σ (front and side views), mesh contour: 3σ].

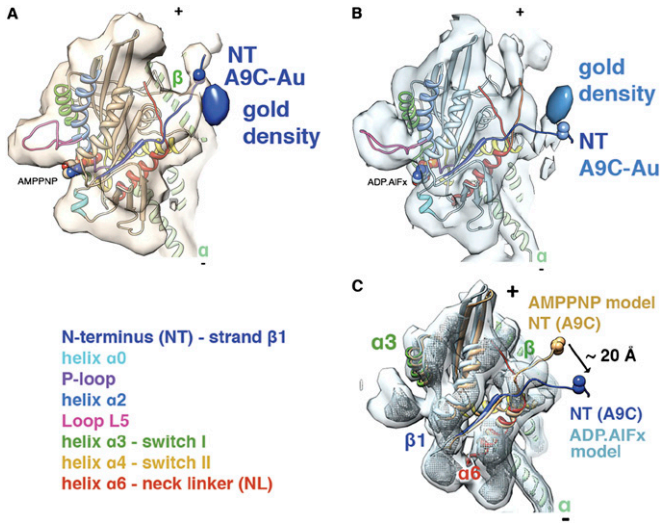

Fig. S5. K5 N terminus gold labeling (A9C) in the AMPPNP and ADP.AlFx states. (*A* and *B*) Difference maps of gold densities (gold covalently attached to the N terminus via A9C) are superimposed onto the native cryo-EM reconstruction (contoured as in Fig. S3) in which pseudoatomic models are docked (color-coded as in the key). Residues A9C are shown in space-filling representation, and gold densities are contoured at 2.2σ (*A*, AMPPNP, dark blue) and 2.3σ (*B*, ADP.AlFx, light blue). (*C*) AMPPNP and ADP.AlFx models are superimposed on helices α4 and docked into the ADP.AlFx reconstruction. The surface is contoured at 2σ; for clarity, only some of the secondary structural elements are shown. The ~20-Å displacement of the N terminus upon ATP hydrolysis is estimated based on the position of the residues A9C (space-filling representation).

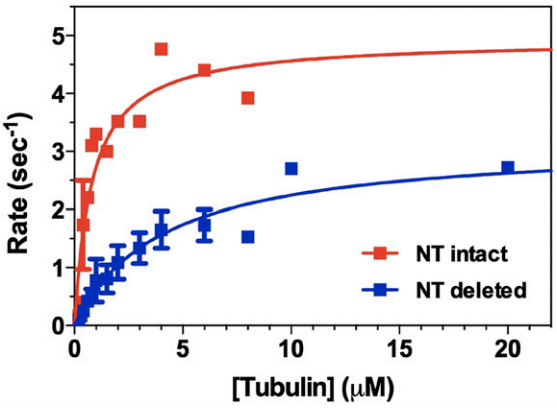

Fig. S6. The effect of the deletion of the N terminus on kinetic parameters of the human K5 ATPase cycle. Steady-state MT-activated ATPase activities of the NT-Intact and NT-Deleted constructs. The reaction was initiated by adding ATP to 2 mM. The dependence of measured rate of inorganic phosphate production on [MT] was fitted to a Michaelis–Menten relationship, defining values of k_{cat} and $K_{0.5,MT}$ of 4.9 ± 0.5/s and 0.81 ± 0.26 μM, respectively, for NT-Intact and 3.2 ± 0.4/s and 4.1 ± 1.1 μM, respectively, for NT-Deleted.

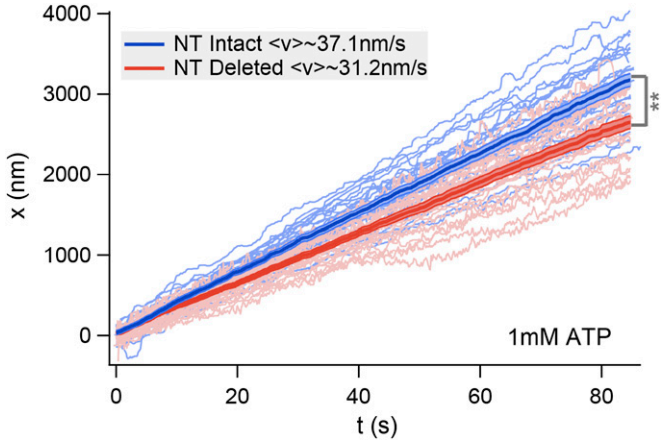

Fig. S7. Effect of deletion of the human K5 N terminus on gliding motility. Individual MT gliding traces for NT-Intact (blue) and NT-Deleted (red) constructs in the presence of 1 mM ATP. Each set of traces ($n = 31$ and 27, respectively) were averaged together pointwise to extract average behavior. [Bold traces: blue, 37.1 nm/s; red, 31.2 nm/s; error bars (light-colored zones) indicate SEM; $^{**}P < 0.001$]. In this trial, neither the NT-Deleted nor NT-Intact samples had a significant number of paused MTs.

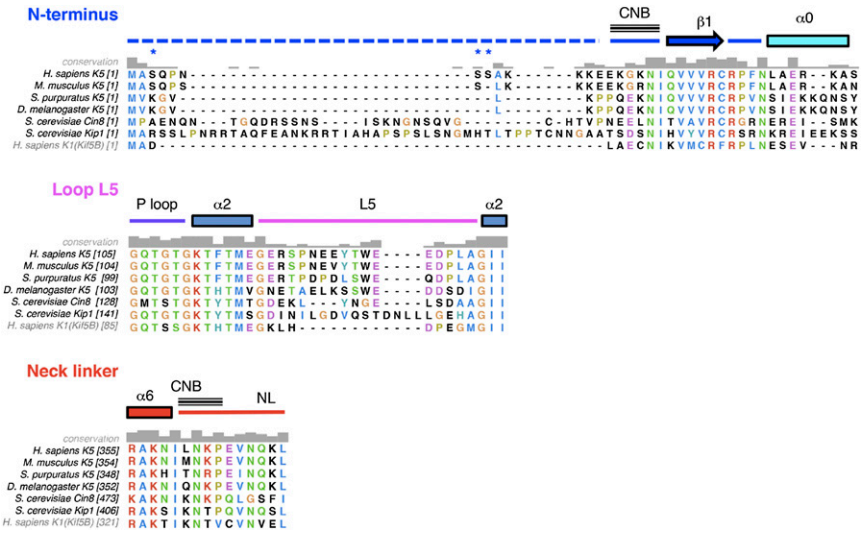

Fig. S8. Sequence comparison between K5/K1 MDs illustrating conservation and divergence of the key regulatory regions. The associated secondary structural elements are indicated above the sequences. The parts of the N terminus and NL involved in cover neck bundle formation (CNB) are indicated. Conserved regions include β1 (blue), the P loop (purple), most of α2 (gray blue), and the C-terminal end of α6 (red). Regions of sequence divergence among K5s and compared with K1 (labeled in gray) are the N terminus (blue), α0 (cyan), L5 (pink), and neck linker (red). UniProt codes are *Homo sapiens* K5: P52732; *Mus musculus* K5: Q6P9P6; *Strongylocentrotus purpuratus* K5: Q9GQ58; *Saccharomyces cerevisiae* Cin8: P27895; *S. cerevisiae* Kip1: P28742; *H. sapiens* K1/Kif5B: Q6P164. The numbers in brackets are the starting residues for each alignment segment. Blue asterisks indicate residues in the N terminus of human K5 that are predicted phosphorylation sites [GPS 2.1 Online (1); NetPhosK1 (2)]. The alignment was generated using T-coffee (3) and displayed using Chimera (4).

1. Xue Y, et al. (2008) GPS 2.0, a tool to predict kinase-specific phosphorylation sites in hierarchy. *Mol Cell Proteomics* 7(9):1598–1608.
2. Blom N, Sicheritz-Pontén T, Gupta R, Gammeltoft S, Brunak S (2004) Prediction of post-translational glycosylation and phosphorylation of proteins from the amino acid sequence. *Proteomics* 4(6):1633–1649.
3. Notredame C, Higgins DG, Heringa J (2000) T-Coffee: A novel method for fast and accurate multiple sequence alignment. *J Mol Biol* 302(1):205–217.
4. Pettersen EF, et al. (2004) UCSF Chimera—a visualization system for exploratory research and analysis. *J Comput Chem* 25(13):1605–1612.

Table S1. Resolution and number of asymmetric units included in each cryo-EM reconstruction

Nucleotide state	K5 sample	No. of asymmetric units (no. of MTs)	Resolution, Å, FSC 0.5
ADP.AlFx	Unlabeled	~139,000 (167)	9.2
	T126C-Au	~7,300 (10)	19
	V365C-Au	~13,000 (13)	16
	A9C-Au	~14,000 (20)	18
ADP	Unlabeled	~125,000 (213)	10
	T126C-Au	~13,000 (26)	18
	V365C-Au	~30,000 (49)	20
	A9C-Au	~14,000 (27)	18
AMPPNP	A9C-Au	~21,000 (31)	25
Rigor	A9C-Au	~18,000 (17)	18

Table S2. Correlation values between the experimental and simulated maps for each K5 MD atomic model

	Correlation values	
Models	ADP.AlFx	ADP
Initial models		
αβ-tubulin (1JFF) +3HQD (AMPPNP)	0.654	0.764
αβ-tubulin (1JFF) +1Il6 (ADP)	0.640	0.768
αβ-tubulin (1JFF) +2WOG (ADP+drug)	0.648	0.767
αβ-tubulin (1JFF) +1Q0B (ADP+drug)	0.642	0.767
Final models	0.673 (NL docked)	0.791
	0.671 (NL undocked)	—

— indicates that only a single final model for the ADP state was calculated.

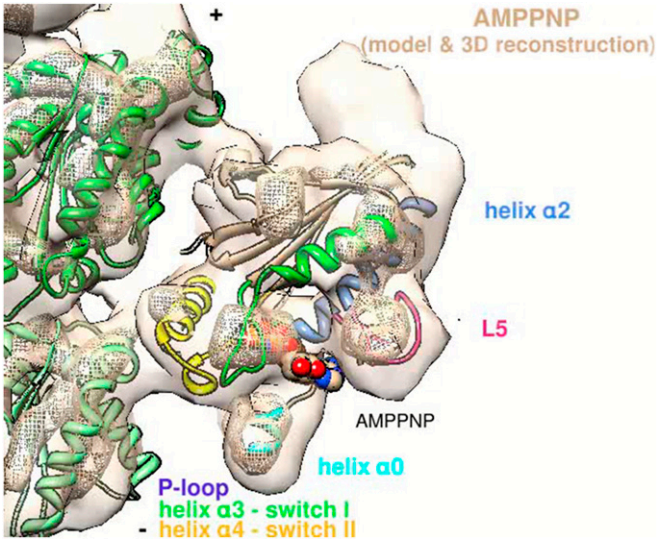

Movie S1. Concerted movement of L5, NL, and N terminus throughout the K5 ATPase cycle: the ATP hydrolysis transition step.

Movie S1

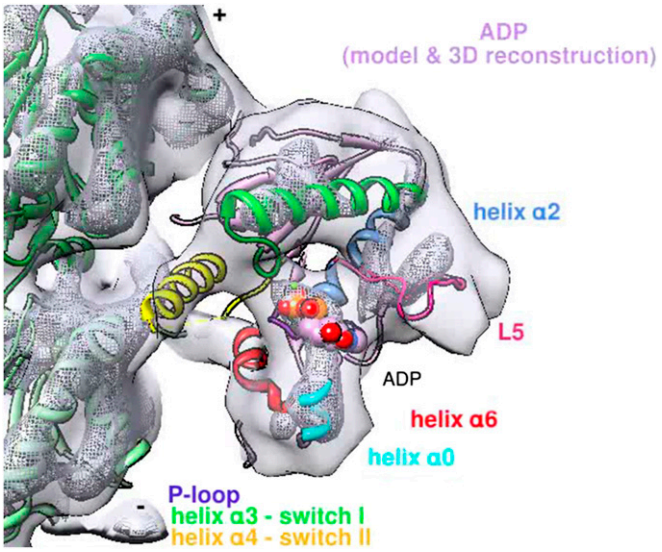

Movie S2. Concerted movement of L5, NL, and N terminus throughout the K5 ATPase cycle: the ADP release step.

Movie S2

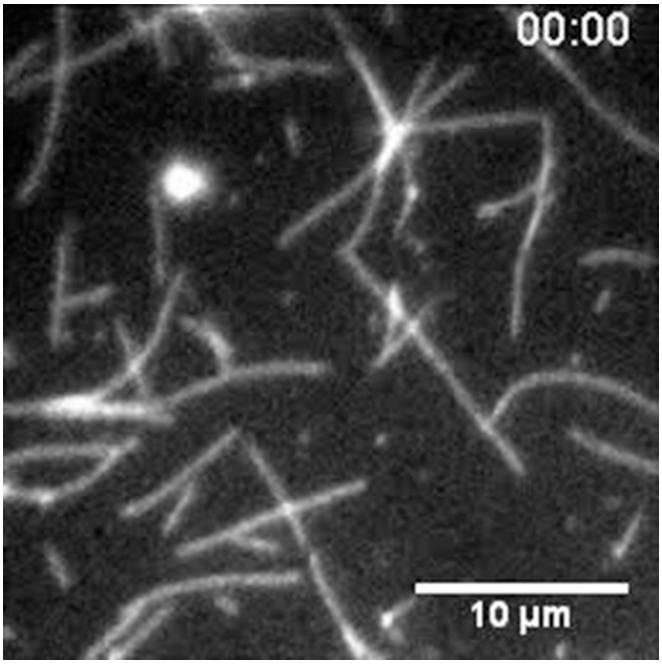

Movie S3. Gliding assay of the NT-Intact K5 MD. MTs are recruited and moved by the NT-Intact K5 MD. The original recording was 512 × 512 pixels, and 11.8 FPS. To make motion obvious, the movies have been sped up and now are viewed at ~0.7 FPS. Because of size considerations, movies for demonstration were down-sampled to 256 × 256 pixels, although actual quantitation as presented in the text was performed on the full-size, full-frame-rate movies.

Movie S3

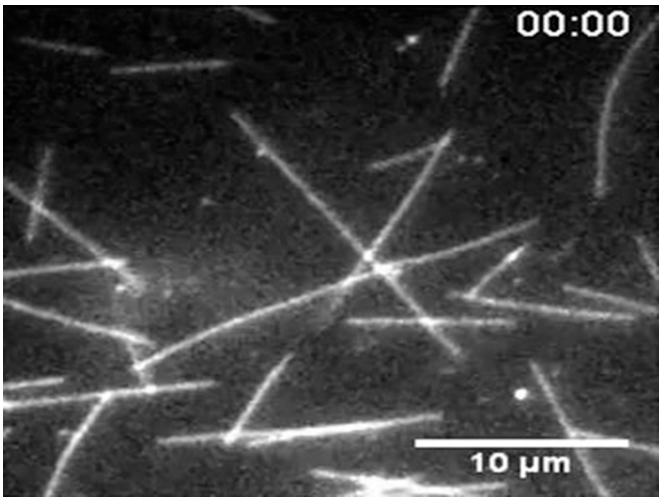

Movie S4. Gliding assay of the NT-Deleted K5 MD. MTs are recruited and moved by the NT-Deleted K5 MD. Movie was prepared as for Movie S3.

Movie S4